Estimator for Charge Acceptance of Lead Acid Batteries

U. Christen, P. Romano, E. Karden

▶ **To cite this version:**

U. Christen, P. Romano, E. Karden. Estimator for Charge Acceptance of Lead Acid Batteries. Oil & Gas Science and Technology - Revue d'IFP Energies nouvelles, 2012, 67 (4), pp.613-631. ⟨10.2516/ogst/2012007⟩. ⟨hal-01936506⟩

HAL Id: hal-01936506

https://hal.science/hal-01936506v1

Submitted on 27 Nov 2018

HAL is a multi-disciplinary open access archive for the deposit and dissemination of scientific research documents, whether they are published or not. The documents may come from teaching and research institutions in France or abroad, or from public or private research centers.

L'archive ouverte pluridisciplinaire **HAL**, est destinée au dépôt et à la diffusion de documents scientifiques de niveau recherche, publiés ou non, émanant des établissements d'enseignement et de recherche français ou étrangers, des laboratoires publics ou privés.

HAL Authorization

© Shutterstock, article DOI: 10.2516/ogst/2012029

Dossier

This paper is a part of the hereunder thematic dossier published in OGST Journal, Vol. 67, No. 4, pp. 539-645 and available online here

Cet article fait partie du dossier thématique ci-dessous publié dans la revue OGST, Vol. 67, n°4, pp. 539-645 et téléchargeable ici

DOSSIER Edited by/Sous la direction de : **A. Sciarretta**

Electronic Intelligence in Vehicles

Intelligence électronique dans les véhicules

Oil & Gas Science and Technology – Rev. IFP Energies nouvelles, Vol. 67 (2012), No. 4, pp. 539-645
Copyright © 2012, IFP Energies nouvelles

Oil & Gas Science and Technology – Rev. IFP Energies nouvelles, Vol. 67 (2012), No. 4, pp. 613-631
Copyright © 2012, IFP Energies nouvelles
DOI: 10.2516/ogst/2012007

Dossier
Electronic Intelligence in Vehicles
Intelligence électronique dans les véhicules

Estimator for Charge Acceptance of Lead Acid Batteries

U. Christen, P. Romano and E. Karden

Ford Forschungszentrum Aachen, Süsterfeldstrasse 200, 52072 Aachen - Germany
e-mail: uchriste@ford.com - paolo.romano@epfl.ch - ekarden@ford.com

Résumé — Estimateur d'acceptance de charge des batteries Pb-acide — Un modèle phénoménologique des batteries plomb-acide est développé et utilisé pour réaliser un estimateur d'acceptance de charge à court terme. Conceptuellement, le modèle est basé sur une équation différentielle partielle qui est discrétisée pour simplifier. La prédiction des états du modèle est améliorée par l'utilisation d'observateurs du courant et de la charge de la batterie. Comme le modèle est essentiellement linéaire, la prédiction à court terme peut être formulée en forme close. Il n'est donc plus nécessaire d'avoir recours à des simulations complexes à chaque instant d'échantillonnage. La seule dépendance non-linéaire, celle à la température, peut être incorporée dans un modèle linéaire à paramètre variable.

Abstract* — *Estimator for Charge Acceptance of Lead Acid Batteries — *A phenomenological model of lead acid batteries is developed that is then used to construct an estimator for short term charge acceptance. Conceptually, the model is based on a partial differential equation that is discretized for tractability. With observers for the battery current and state of charge, the prediction of the internal states is improved. Since the model is essentially linear, the short term prediction can be implemented in closed form, thus without the need for computationally intensive prediction simulations at each sampling instant. The only nonlinearity, the dependence on temperature, can be incorporated in a linear parameter-varying model.*

INTRODUCTION

Automotive batteries that are important for the propulsion of the vehicle are monitored with a Battery Monitoring System (BMS). For Micro-Hybrids, *i.e.*, hybrid electric vehicles with stop-start functionality, the battery is either a flooded or an Absorptive Glass Mat (AGM) lead acid battery. Today's BMS for these kinds of batteries monitors parameters like State of Charge (SOC, percentage of maximum charge that is stored) and state of health (percentage of nominal capacity that is still available for storing charge). However, the maximum current with which the battery could be charged at a given voltage is not assessed. Unlike for other battery chemistries, this charge acceptance of lead acid batteries strongly depends on the charge and discharge history the battery has gone through. Knowing the charge acceptance would allow to save fuel by charging the battery only in opportune situations.

There has been quite some activity in modeling batteries in the past but many of them deal with other chemistries than lead acid (see, *e.g.*, [1] for a recent overview). For lead acid batteries, there are two basic approaches to modeling: based on the electrochemical phenomena (*e.g.*, [2-4]) or as a phenomenological model (*e.g.*, [5, 6]). Such phenomenological models, which usually contain one or two RC elements (possibly with an additional input resistance), are often used for SOC estimation; they are frequently combined with an (extended) Kalman filter (*e.g.*, [7]). In this paper, we develop a phenomenological model as well since it needs to be sufficiently simple for real-time execution in an automotive

embedded controller. However, in order to be able to predict charge acceptance (as opposed to SOC alone), we need more than just two time constants and thus a structure involving more than two RC elements.

This paper is organized as follows. In the next section, the background of the model is set by sketching the phenomena the model should cover and describing a conceptual model. Section 2 introduces the phenomenological model, covering both, the model structure and parameters identified. In Section 3, the results obtained with the model are improved by observers that feed back measured values for the outputs. In Section 4, the actual estimation of the charge acceptance is covered. The last section contains the description of how the nonlinear temperature dependence can be incorporated to form a linear parameter varying model.

1 BACKGROUND

Lead acid batteries are notorious for being hard to recharge if they have been resting for a while after discharge. Their charge acceptance strongly depends on the charge and discharge history: if the battery has recently been discharged with a high current, it is easy to restore the removed charge with a high current. But once the charge just taken out is replaced, the charge acceptance rapidly decreases and further charging has to be done at a rather low current (at least without exceeding safe voltage limits), as if some arteries got clogged if they are not exercised sufficiently.

Today's Battery Monitoring Systems (BMS) for lead acid batteries measure the voltage across the battery, the current entering or leaving the battery and the temperature of the battery. With this information and a few parameters (such as nominal battery capacity), the BMS monitors, among others, the State of Charge (SOC) and the State of Health (SOH) of the battery. SOC essentially involves the integration of the battery current to keep track of the charge in the battery; in order to deal with bias, the SOC can be reset based on the open circuit voltage after long rest periods (times without battery activity, *e.g.*, if the vehicle has not been driven over night or during a weekend). State of Charge describes the percentage of the capacity the battery currently has that is filled with charge. State of Health, on the other hand, describes the percentage of the nominal battery capacity that is still available currently ([8, 9]). The available capacity reduces over the lifetime of a battery.

For SOC assessment, a rather simple dynamic model is sufficient: an integrator for the current. (Some logic is needed for occasionally resetting the effects of bias.) For the description of charge acceptance limitations, a more elaborate model is needed. However, in order to keep the model relatively simple such that it can be used for an observer design or an implementation in electronic control units, we are not developing a model of the chemical and physical processes taking place in the battery but a phenomenological model. In the remainder of this background section, we thus describe the phenomena that should be captured by the model and then a conceptual model in the form of a partial differential equation.

1.1 Phenomena to Be Covered

In a vehicle, the battery experiences different modes of operation. During discharge, consumers usually draw some given current. From a modeling point of view, this looks like a current driven operation: a current is imposed and the voltage is the response of the battery.

During charging, the voltage of the generator is controlled to a value above the open circuit voltage of the battery in order to impose some charging current. For moderate charging during times of good charge acceptance, such a current (or power) driven charging is possible. However, when the charge acceptance decreases or charging with very high power is desired, the voltage would exceed safe bounds. Thus, the charging no longer is current or power driven but the maximum voltage that safely can be applied is used. The battery thus sees a voltage driven operation.

There is an additional constraint in the vehicle. Changes in voltage should not be too fast because the driver can see voltage changes in the brightness of lights, for instance. During the voltage ramping, the battery would also see voltage driven operation.

In the following, we list a few phenomena observed with lead acid batteries:

- the predominant property of the battery is its ability to store (and release) charge; essentially, it is a charge balancing device. Even though this is already captured in today's BMS, our model needs to respect it as well;
- the most prominent phenomenon observed during charging is the seemingly exponential decrease of the current over time if the battery is charged with constant voltage *(Fig. 1)* or, conversely, the increase of the voltage over time that is needed to charge the battery with a constant current. This visualizes the charge acceptance problem with lead acid batteries. The trends are the same for flooded and AGM batteries but the values may be different;
- the same can be observed during discharging. During discharge with constant current, the battery voltage reduces approximately exponentially over time *(Fig. 2)*. Similarly, the magnitude of the current would decrease if the battery was connected to a constant voltage below the open circuit voltage – difficult to do experimentally, though;
- charge acceptance is not only time dependent. There is an additional dependence on the State of Charge. For the same voltage, the charging current is higher for lower SOC, as seen in Figure 3;
- however, even for the same SOC, the charge acceptance depends on the charging and discharging history. If the

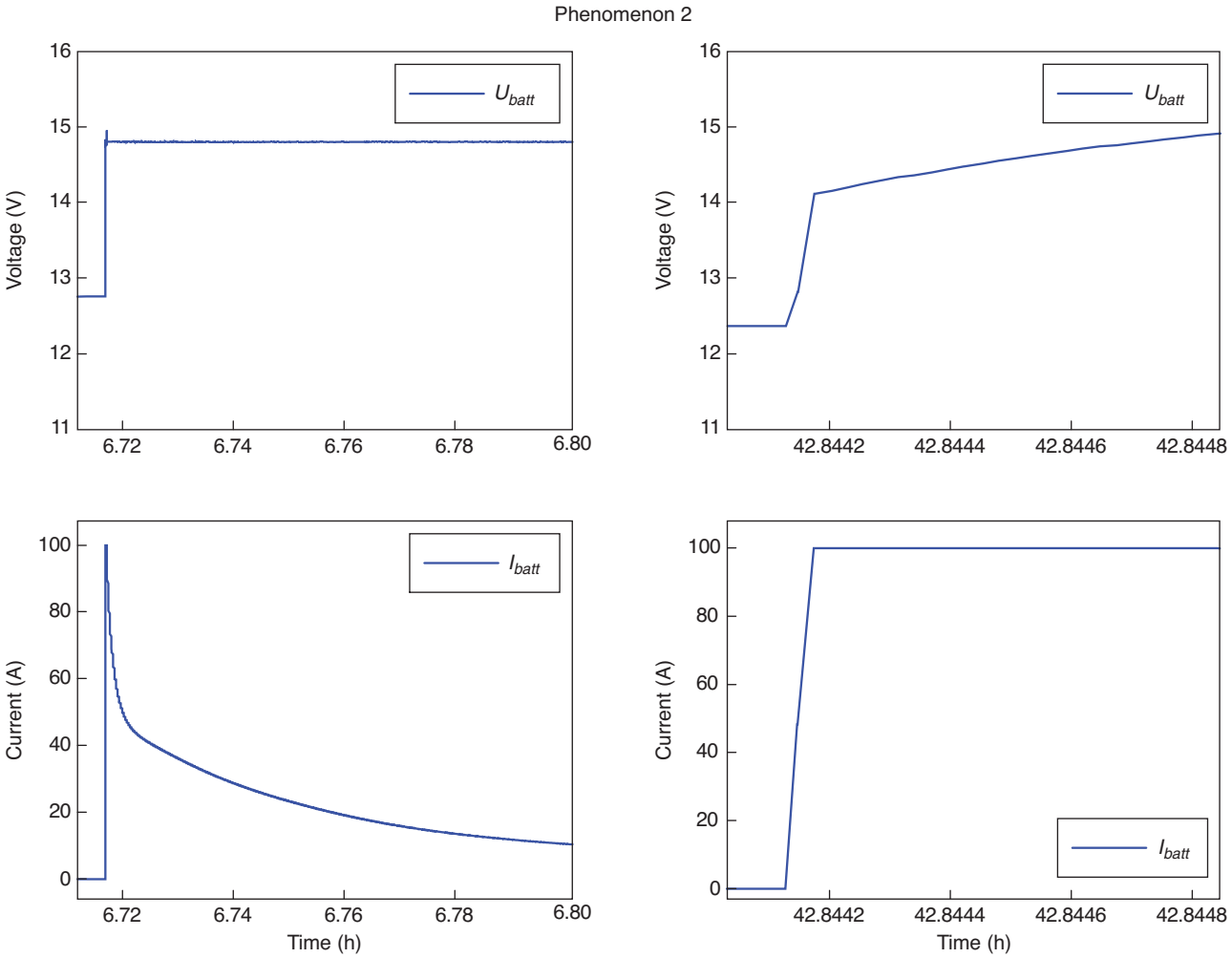

Figure 1

Phenomenon 2 – Exponential decrease of current during charging with constant voltage and increase of voltage during charging with constant current.

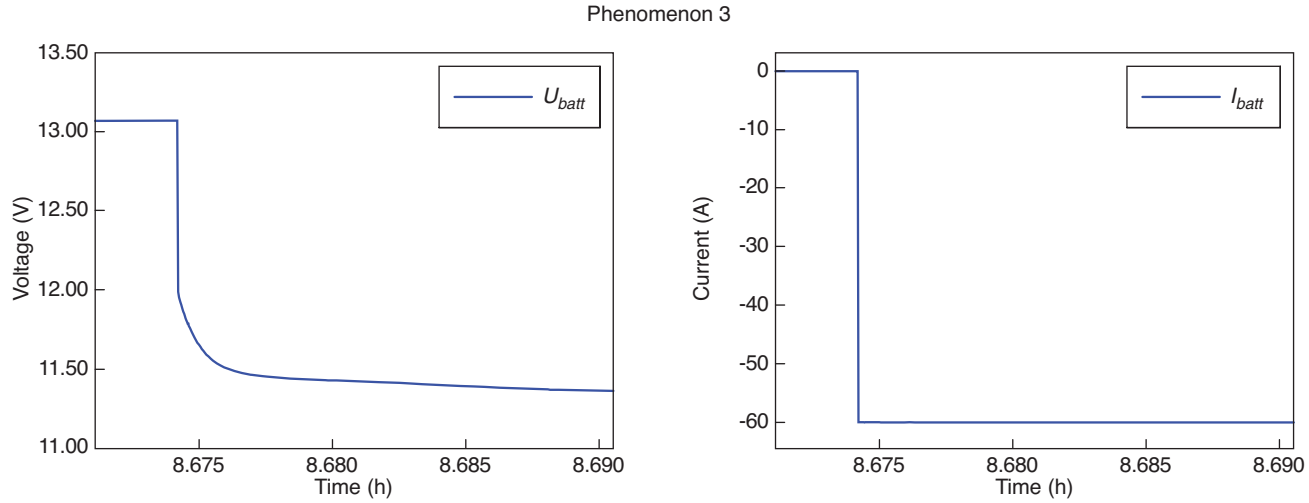

Figure 2

Phenomenon 3 – Exponential decrease of voltage during discharging with constant current.

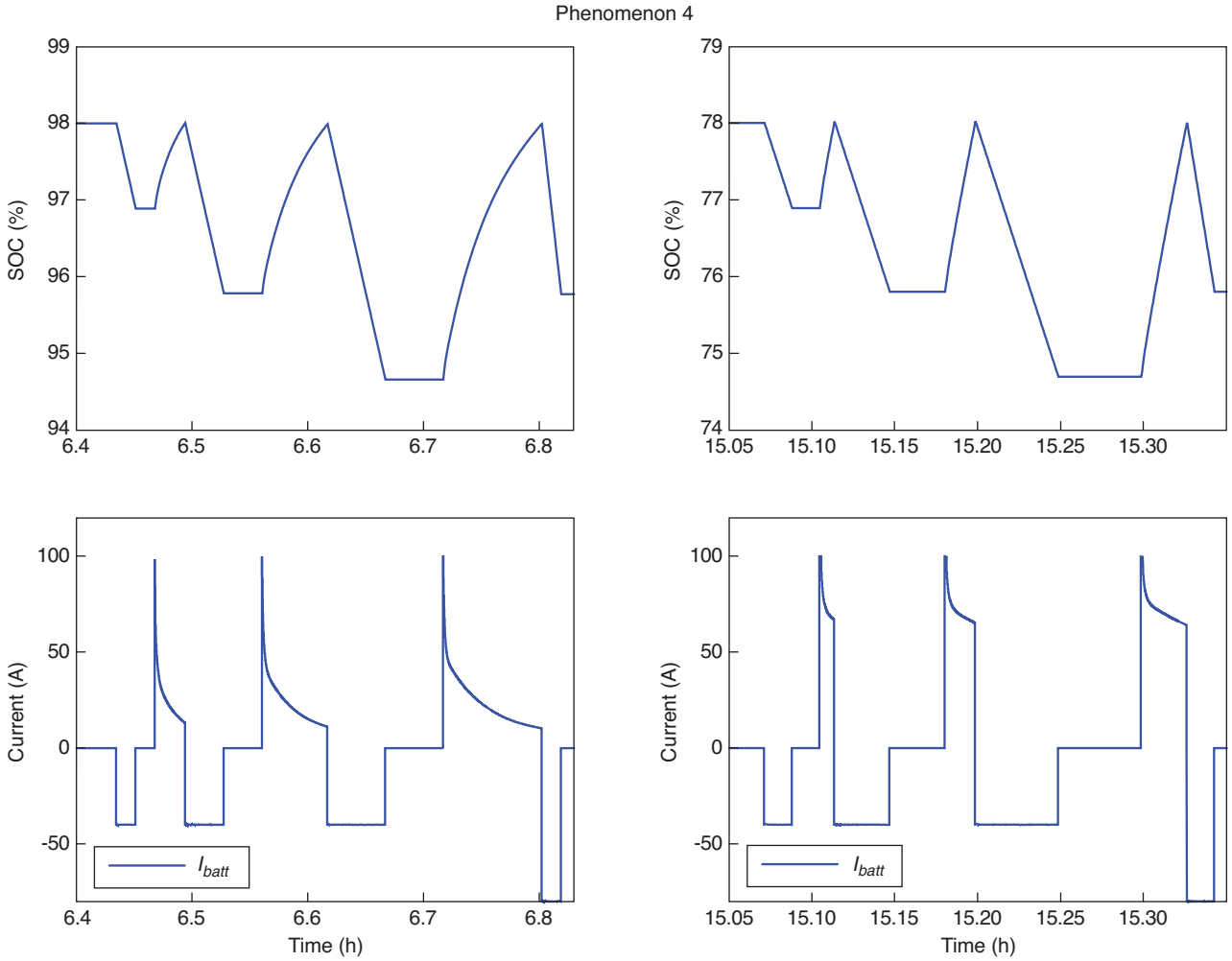

Figure 3

Phenomenon 4 – SOC dependence of the charging current.

battery has been discharged to reach a certain SOC, the charge acceptance is much higher than if the same SOC has been reached by charging *(Fig. 4)*. This is a phenomenon reminiscent of hysteretic behavior;

– this dependence on previous history can also be seen by varying the rest period between discharging and charging, as in Figure 5. The longer the rest period after discharge, the lower the current that is accepted. This is consistent with the trends seen as Phenomenon 2 as well;

– the battery parameters are temperature dependent (see, *e.g.*, [8]). At temperatures close to freezing, a battery essentially does not accept any significant charging current. With decreasing temperature the internal resistance of the battery increases such that higher voltage differences are needed to charge or discharge the battery with a defined current. Thus, the lower threshold indicating an empty battery is reached earlier, leading to an apparently smaller capacity of the battery;

– as the battery ages, its capacity gets reduced. This is captured with the State of Health (SOH);

– when a battery is fully charged (SOC reaches 100%), gassing occurs with some batteries – current goes into hydrolysis rather than charge storage. Gassing is not a major issue anymore but charge acceptance is still limited.

1.2 Conceptual Model

If just the first three or four phenomena listed above would have to be captured, a relatively simple model with one or two RC elements would be sufficient. In order to describe

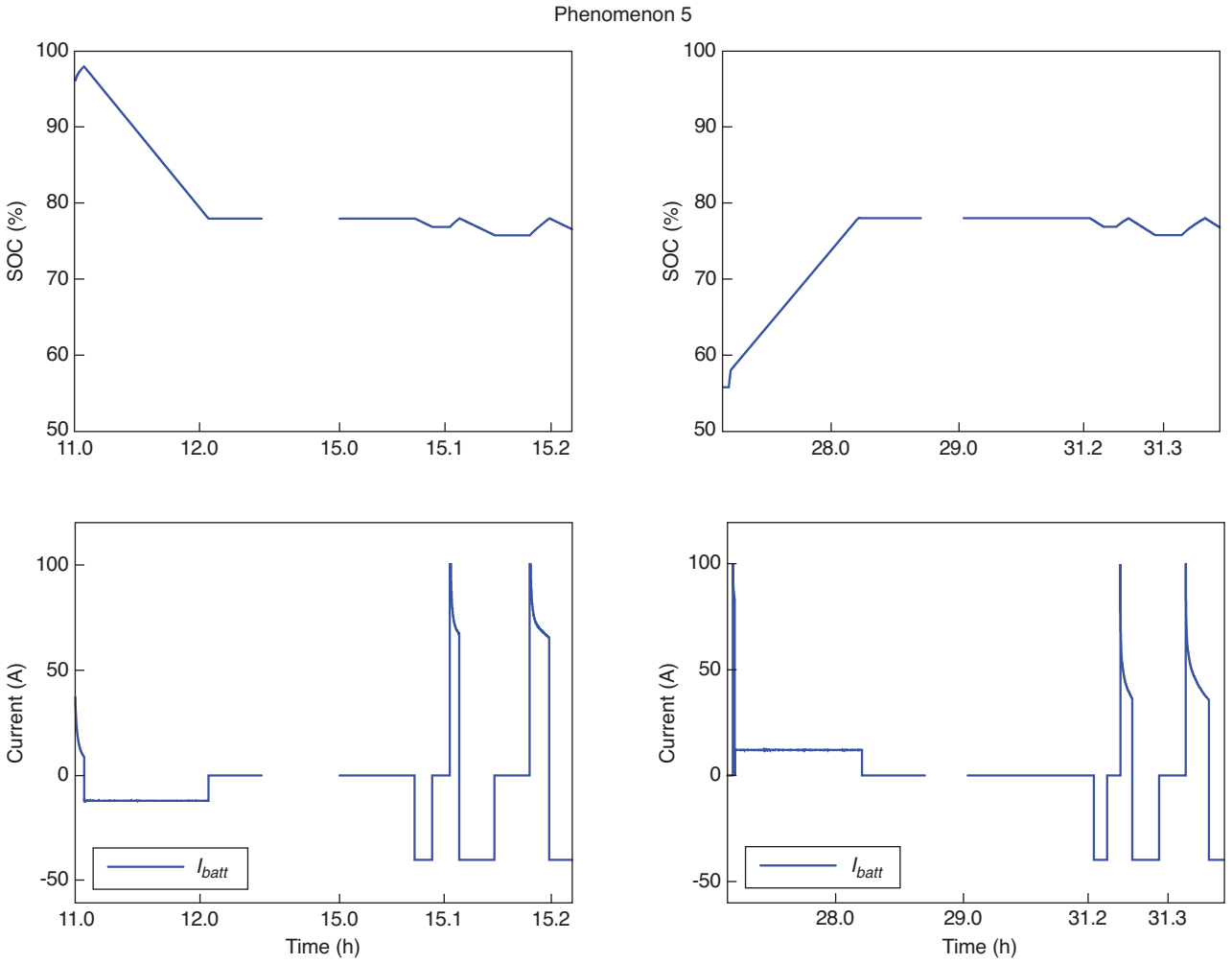

Figure 4

Phenomenon 5 – Charging current depending on charging and discharging history.

some of the other phenomena, additional RC elements could be introduced that store the history. At a closer look, even the exponential response described as Phenomenon 2 involves more than just one or two linear dynamic elements: the curve cannot be reproduced with just a single time constant.

In fact, a high number of time constants spread over a large range is needed to describe it all. The time constants of the fastest phenomena shown above are in the order of seconds. The time constants involving the rest periods can extend to several hours, the history or the hysteretic behavior to several days or weeks. The battery aging then involves time constants in the order of the battery life itself.

Conceptually, the phenomena listed above can be captured by having a continuum of time constants using a partial differential equation describing a spread-out capacitance with varying resistance that impedes the flow of charge:

$$\frac{1}{R(x)}\frac{\partial^2}{\partial x^2}U(t,x) - C(x)\frac{\partial}{\partial t}U(t,x) = 0 \qquad (1)$$

Here x describes some fictitious spacial dimension "along the battery", t the time, U the voltage, R the resistance and C the capacitance as a function of the position "in the battery". A boundary condition is:

$$U(t,0) = U_{batt}(t) \qquad (2)$$

where U_{batt} is the voltage at the poles of the battery.

Equation (1) is the well-known telegrapher's equations specialized for the situation where the inductance and the conductance vanish.

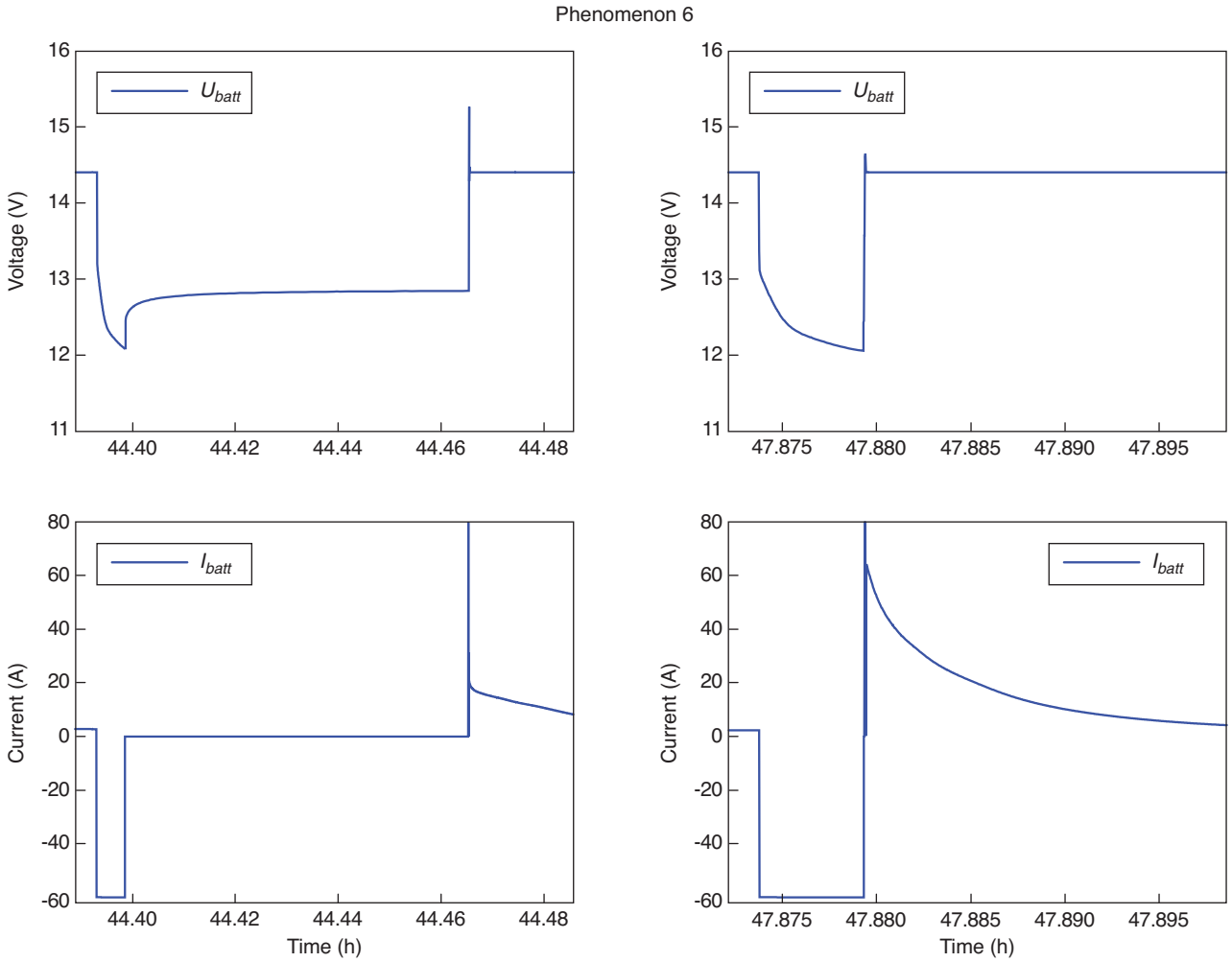

Figure 5

Phenomenon 6 – Charging current depending on history of rest period.

The model can be visualized as sketched in Figure 6. Along the spacial dimension x, there are a spread-out capacitance $C(x)$ and a resistance $R(x)$. The local voltage is denoted as $U(t, x)$, the voltage at the poles as U_{batt}; I_{batt} is the current.

Figure 6 also shows a hydraulic analogon that helps with the interpretation (especially for mechanical engineers): the battery visualized as a water tank. Voltage is replaced by the level h, current by the flow f. The equivalent for the capacitance is the porosity of the material in the tank, that for resistance is its permeability.

The development of the local voltage over time is illustrated in Figure 7. At the battery poles (position 0), the variation of the voltage is high while at the other end (position 6), it essentially remains constant for the excitation shown here.

There is some redundancy in this model. Instead of changing C with x, longer or shorter sections with constant C (and different $R(x)$) could be taken. Alternatively, R could be constant and only C varied with x. With the discretization of the model in the next section, this becomes irrelevant, however. All parameters are lumped anyway.

Temperature dependence of the parameters has not been introduced so far. However, as noted above (Phenomenon 7), everything depends on temperature such that R (and possibly C) should be understood to depend on temperature ϑ:

$$R(x, \vartheta),\ C(x, \vartheta) \tag{3}$$

This model conceptually captures Phenomena 1 through 7 but not 8 and 9. We neglect Phenomenon 8 (aging) in the model and deal with it in the observer section. Similarly, Phenomenon 9 (gassing) is neglected since the battery will be operated below full of charge anyway.

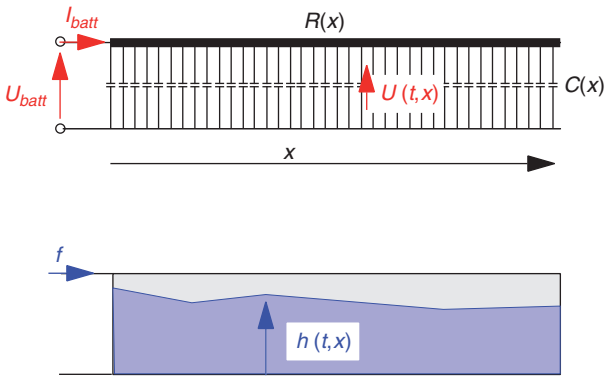

Figure 6

Visualization of the conceptual battery model.

2 PHENOMENOLOGICAL BATTERY MODEL

2.1 Model Structure

Partial differential equations are not practical for implementation. The x axis is discretized such that the parameters and quantities spread out along this axis are lumped into discrete values, as illustrated in Figure 8. $C(x)$ and $R(x)$ each are lumped into n discrete values, C_i and R_i. The hydraulic analogon would be a tank with n compartments, each with a capacity corresponding to C_i and walls with a permeability corresponding to R_i. The levels h_i in the compartments correspond to the voltages U_i of the capacitors.

In general, the compartments do not correspond to the cells of a battery. As discussed above, we need to model a large range of time constants and we want to do this with a minimum number of differential equations or compartments. We thus choose a non-uniform partitioning of the battery. For capturing fast phenomena, we need small compartments placed at the "beginning" (near the poles) of the battery. For the slow phenomena, we can have large compartments at the end of the battery. This is visualized in Figure 8.

This RC network can be described with a set of n ordinary differential equations:

$$\dot{U}_i = \frac{1}{C_i}\left(\frac{U_{i-1} - U_i}{R_i} - \frac{U_i - U_{i+1}}{R_{i+1}}\right) \quad i = 1, \ldots, n \tag{4}$$

with $U_0 = U_{batt}$, $U_{n+1} = 0$, $R_{n+1} = \infty$ (alternatively, R_{n+1} could be set to a value describing self-discharge of the battery).

Together with the output equation:

$$I_{batt} = \frac{U_{batt} - U_1}{R_1} \tag{5}$$

this describes the situation when the voltage at the battery poles is imposed. If the current is imposed rather than the voltage, the first differential equation needs to be changed since the current through R_1 is given:

$$\dot{U}_1 = \frac{1}{C_1}\left(I_{batt} - \frac{U_1 - U_2}{R_2}\right) \tag{6}$$

and the output equation then reads:

$$U_{batt} = U_1 + R_1 I_{batt} \tag{7}$$

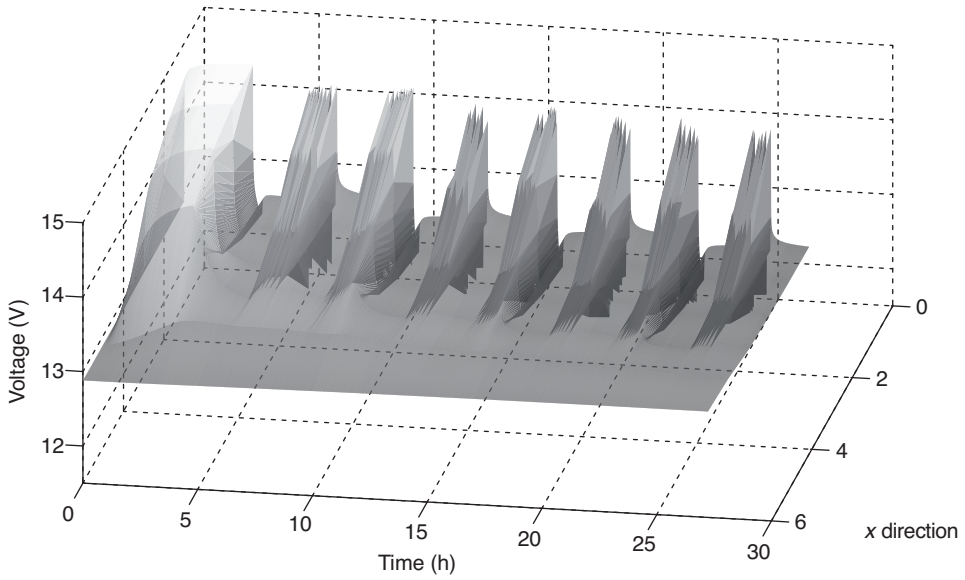

Figure 7

Voltage over time "along" the battery.

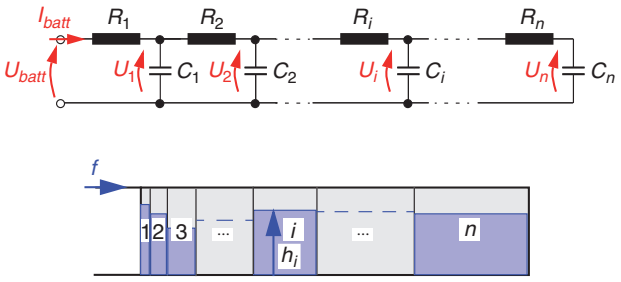

Figure 8

Discretized battery with n compartments.

Except for the switching of the input and the output depending on the operating regime, Equations (4) to (7) describe a linear system with, depending on n, high order but a lot of structure. The dynamics matrix implied by Equation (4) is a tri-diagonal sparse matrix:

(see *Eq. 8)*

Vectorized, this can be written as:

$$\dot{U} = AU + BU_{batt} \tag{9}$$

and similarly for the model with I_{batt} as the input.

2.2 Analysis of the Model

The model has different behavior depending on whether the current or the voltage is chosen as input. In both cases, the model is stable, as the poles and zeros for the model with eight compartments show *(Tab. 1)*. The nonminimum phase zero is a numerical artifact; it should be at 0 exactly. The magnitude Bode plots for the two models *(Fig. 9)* illustrate the difference between them. With current as input, the model is predominantly integrating (low pass behavior); it is well apt to capture longer-term trends – most obviously the integration of current to reflect SOC. With the voltage input, the model shows high pass behavior that is more suitable for capturing short term effects such as charge acceptance. With the use of observers (see below), the two behaviors can be blended.

As some sort of a summary, Figure 10 shows the effects of several phenomena when the charging voltage is changed during charging. Initially, the charge acceptance exceeds the maximum current the charging device can provide such that the battery is charged with constant current and increasing voltage until the voltage setpoint is reached. This phase is followed by charging with constant, high voltage (14.8 V). At the switching from the higher to the lower charging voltage (13.8 V), the current first needs to be brought to 0 A; once the desired voltage is applied, the charging current is increasing (rather than decreasing as usually) because the voltage at the poles is very close to the new charging voltage such that the voltage difference driving the charging is small. First, the battery internal charge needs to be distributed (the voltage needs to be distributed) before the current can increase *(Fig. 11)*; after having increased, the charging current drops again as the filling of the "compartments" close to the poles increases. When the charging voltage is switched back to the higher voltage, the driving difference is larger again and hence the charging current is initially large again and then decreases exponentially.

2.3 Parameters

The nominal capacity of the battery, Q_{nom}, indicates the charge that can be removed from the battery if it is discharged with I_{20}, *i.e.*, a current that removes 1/20 of the nominal capacity per hour, until the minimum voltage is reached. During this operation, the open circuit voltage drops from the maximum value at fully charged battery, $U_{oc,\max}$, to the minimum value at completely discharged battery, $U_{oc,\min}$. The total capacity of the battery, C_{batt}, is then calculated as:

$$C_{batt} = \frac{Q_{nom}}{U_{oc,\max} - U_{oc,\min}} \tag{10}$$

$$\begin{bmatrix} \dot{U}_1 \\ \dot{U}_2 \\ \vdots \\ \dot{U}_i \\ \vdots \\ \dot{U}_n \end{bmatrix} = \begin{bmatrix} \frac{-1}{C_1}\left(\frac{1}{R_1}+\frac{1}{R_2}\right) & \frac{1}{C_1R_2} & 0 & 0 & \dots & 0 \\ \frac{1}{C_2R_2} & \frac{-1}{C_2}\left(\frac{1}{R_2}+\frac{1}{R_3}\right) & \frac{1}{C_2R_3} & 0 & \dots & 0 \\ 0 & & \dots & & & 0 \\ 0\dots & \frac{1}{C_iR_i} & \frac{-1}{C_i}\left(\frac{1}{R_i}+\frac{1}{R_{i+1}}\right) & \frac{1}{C_iR_{i+1}} & \dots & 0 \\ 0 & & & \dots & & 0 \\ 0 & & \dots & 0 & \frac{1}{C_nR_n} & \frac{-1}{C_nR_n} \end{bmatrix} \begin{bmatrix} U_1 \\ U_2 \\ \vdots \\ U_i \\ \vdots \\ U_n \end{bmatrix} + \begin{bmatrix} \frac{1}{C_1R_1} \\ 0 \\ \vdots \\ 0 \\ \vdots \\ 0 \end{bmatrix} U_{batt} \tag{8}$$

TABLE 1

Poles and zeros of the models

Model with U_{batt} as input		Model with I_{batt} as input	
Zeros	Poles	Zeros	Poles
–1.5725e+000	–2.6912e+000	–2.6912e+000	–1.5725e+000
–4.2443e–001	–6.5822e–001	–6.5822e–001	–4.2443e–001
–1.1747e–001	–1.6803e–001	–1.6803e–001	–1.1747e–001
–3.3718e–002	–4.9537e–002	–4.9537e–002	–3.3718e–002
–6.7367e–003	–9.4911e–003	–9.4911e–003	–6.7367e–003
–1.5891e–003	–2.5115e–003	–2.5115e–003	–1.5891e–003
–5.8169e–005	–2.1918e–004	–2.1918e–004	–5.8169e–005
5.6969e–019	–1.6253e–005	–1.6253e–005	–2.6115e–019

Typical values for flooded and AGM batteries are shown in Table 2.

TABLE 2

Typical values for AGM and flooded batteries

Battery type	Q_{nom}	$U_{oc,\max}$	$U_{oc,\min}$	C_{batt}	$R_{1,\max}$	$C_{1,\max}$
	(Ah)	(V)	(V)	(kF)	(mΩ)	(kF)
AGM	70	12.91	11.56	187.08	7	2
Flooded	60	12.88	11.86	211.56	18	2

An upper bound for the resistance of the first compartment can be estimated by looking at the last voltage value

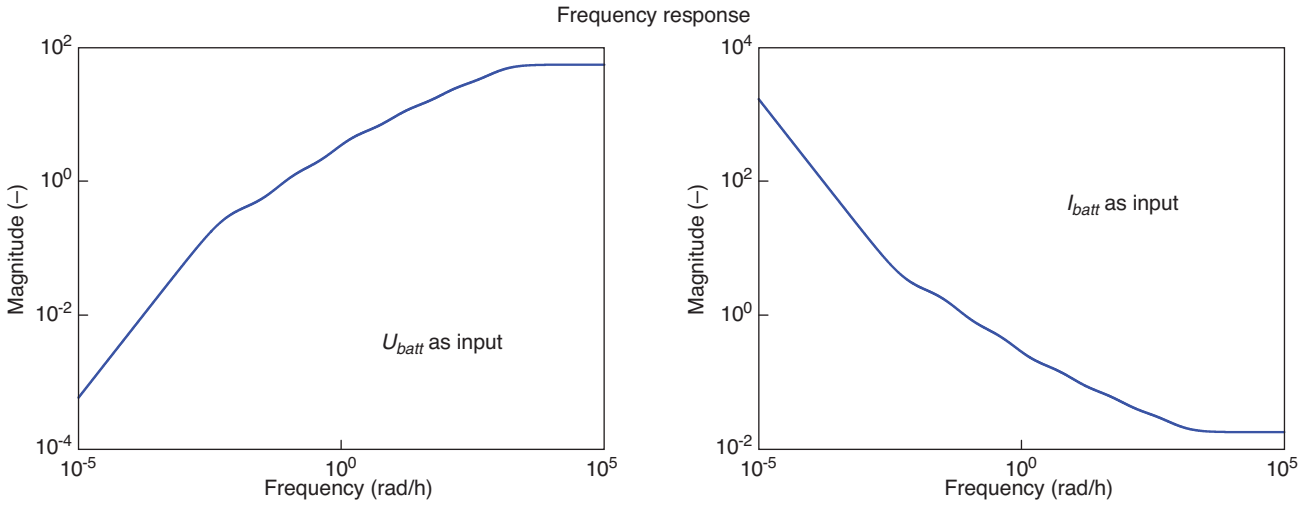

Figure 9

Magnitude Bode plots.

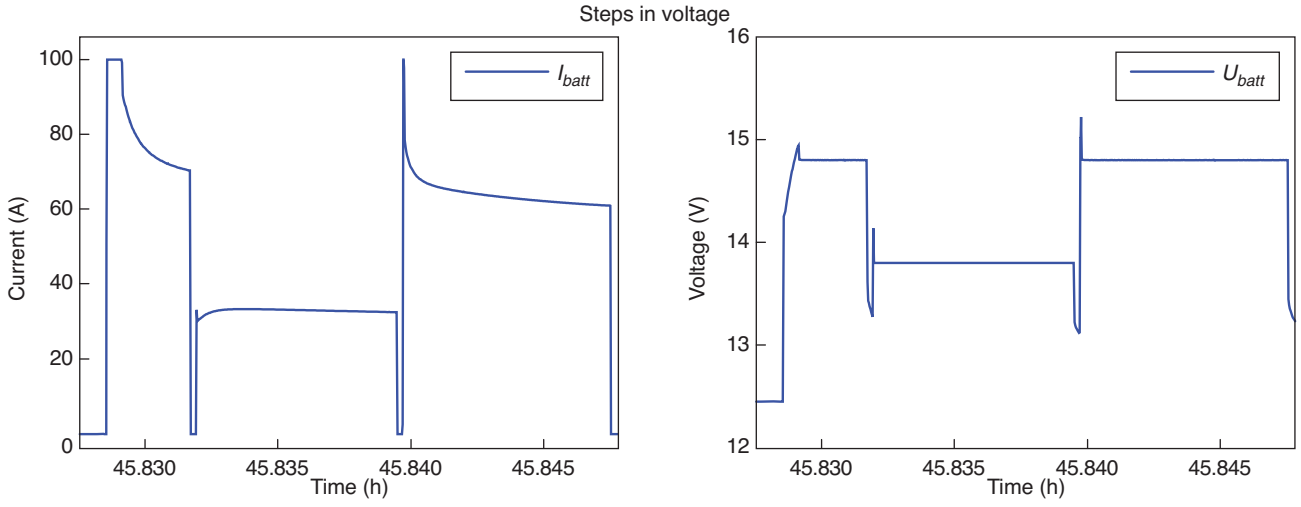

Figure 10

Charging with varying voltage.

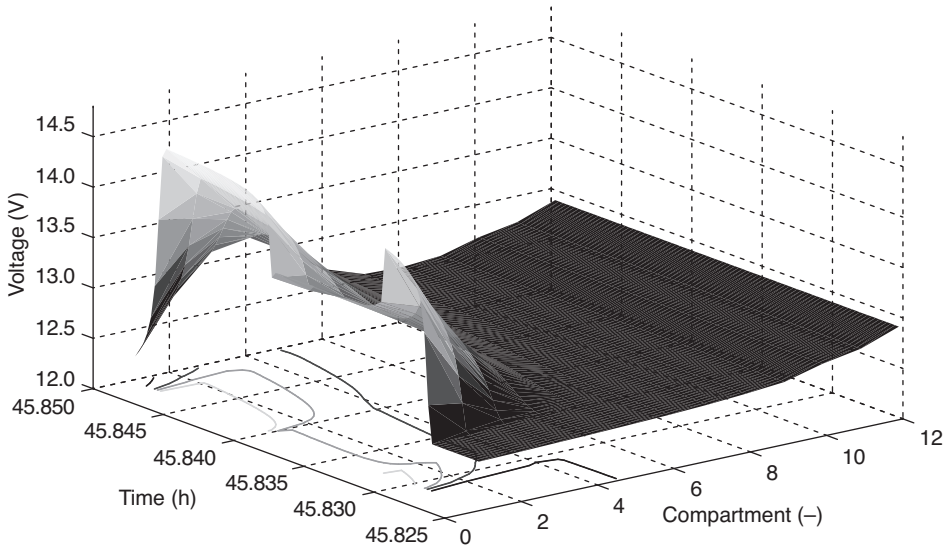

Figure 11

Distribution of voltage inside the model during charging with varying voltage.

measured before and the first voltage value measured after a step change in current from 0 A to either a positive or a negative value. As can be seen from the output equation, Equation (7):

$$R_1 = \frac{U_{batt} - U_1}{I_{batt}} \tag{11}$$

where U_1 cannot be measured directly but it can be approximated by U_{batt} before the step change because $U_1 \approx U_{batt}$ during rest (*i.e.*, $I_{batt} = 0$ A). Since, there is a finite time between the two samples of U_{batt}, the resulting value for R_1 is only an upper bound for the true value. Typical values for the two types of batteries can again be seen in Table 2.

Similarly, a value for the first capacitance can be obtained from the first two voltage samples measured after a current step. The differential equation for the voltage of the first compartment, Equation (6), solved for C_1, reads:

$$C_1 = \frac{1}{\dot{U}_1}\left(I_{batt} - \frac{U_1 - U_2}{R_2}\right) \tag{12}$$

Approximating the derivative and assuming $U_2 \approx U_1$ (with a similar argument as above):

$$C_1 \approx \frac{T_s}{U_1(k+1) - U_1(k)} I_{batt} \tag{13}$$

where T_s is the sampling time and k denotes the sample right after the step change. U_1 is now expressed by the output equation solved for U_1 ($U_1 = U_{batt} - R_1 I_{batt}$) such that, with $I_{batt}(k) = I_{batt}(k+1)$:

$$C_1 \approx \frac{T_s}{U_{batt}(k+1) - U_{batt}(k)} I_{batt} \tag{14}$$

Again, this is an upper bound on the true value.

The number of compartments, n, needs to be chosen in a trade off between representing the relevant time constants and avoiding a stiff system of too high order. The comparison of C_1 with C_{batt} shows that there would be a very high number of compartments if they were chosen equally sized (in the order of 100 compartments). However, we want to cover a broad range of time constants such that the capacities should be chosen with increasing size. Moreover, as discussed in Section Conceptual Model, there is some redundancy in the model that allows for fixing the capacities of the compartments. Reasonable numbers for n are somewhere between 4 and 12.

The sum of all capacities has to be equal to C_{batt}:

$$\sum_{i=1}^{n} C_i = C_{batt} \tag{15}$$

this gives the values shown in Table 3 as reasonable distributions.

Finally, the resistances are chosen by parameter optimization with measured data. The resistances show an increasing trend as well *(Tab. 3)*.

The temperature dependence is introduced by making the resistances temperature dependent. As can be seen in [10] for the internal resistance (equivalent to R_1 introduced here), the dependence may be expressed as a factor *(Fig. 12)*. We apply it to all the resistances:

$$R_i(\vartheta) = (a_3\vartheta^3 + a_2\vartheta^2 + a_1\vartheta + a_0)R_i \tag{16}$$

with $a_3 = -7.292 \times 10^{-7}$ 1/(°C)^3, $a_2 = 1.509 \times 10^{-4}$ 1/(°C)^2, $a_1 = -9.869 \times 10^{-3}$ 1/°C, $a_0 = 1.147$; for $\vartheta_0 = 20$°C, the factor is 1.

TABLE 3

Typical values for C_i and R_i

AGM battery						Flooded battery					
C_i (kF)			R_i (mΩ)			C_i (kF)			R_i (mΩ)		
$n = 4$	$n = 8$	$n = 12$	$n = 4$	$n = 8$	$n = 12$	$n = 4$	$n = 8$	$n = 12$	$n = 4$	$n = 8$	$n = 12$
0.20	0.10	0.052	7.0	7.0	7.0	0.34	0.11	0.052	18	18	18
1.9	0.28	0.10	10	9.4	7.4	2.8	0.31	0.10	32	20	18
18	0.77	0.20	17	9.5	7.4	23	0.84	0.21	130	22	19
167	2.1	0.40	87	12	7.5	186	2.3	0.42	820	26	20
	5.8	0.79		13	7.6		6.4	0.83		51	22
	16	1.6		27	7.8		18	1.7		80	25
	43	3.1		35	8.4		49	3.3		790	30
	119	6.1		390	9.0		135	6.6		970	39
		12			17			13			55
		24			43			26			390
		47			270			53			440
		92			2 500			106			6 200

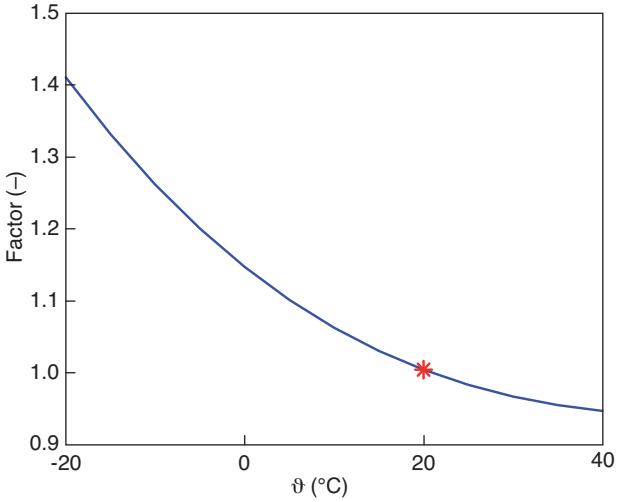

Figure 12

Factor modeling temperature dependence.

2.4 Model Refinements

There are several options for refining the model. One could use different resistance values for the resistors depending on whether the current flowing through them is positive or negative, as visualized in Figure 13. This amounts to having different resistance values for charging and discharging. If the observed time constants for charging and discharging are different, then such different resistance values help to capture the behavior.

A further alternative that may help to reduce the order of the model is to use hysteretic elements for the resistors as defined in [11]. This may help to capture the hysteretic behavior (Phenomenon 5). However, it is not expected to help with the other phenomena.

3 OBSERVERS

Three observers are added to the base model in order to improve the behavior of the charge and discharge capturing. There are two observers to deal with SOC and SOH, respectively and there is one to deal with the measured battery output (battery voltage for the current driven model; current when voltage driven).

3.1 SOC Observer

A State of Charge estimation can be an additional output of the model (4) to (7) described above. SOC is the percentage of the available capacity that is currently used:

$$SOC = \frac{Q - Q_{\min}}{Q_{\max} - Q_{\min}} = \frac{1}{C_{batt}(U_{oc,\max} - U_{oc,\min})} \sum_{i=1}^{n} C_i (U_i - U_{oc,\min}) \tag{17}$$

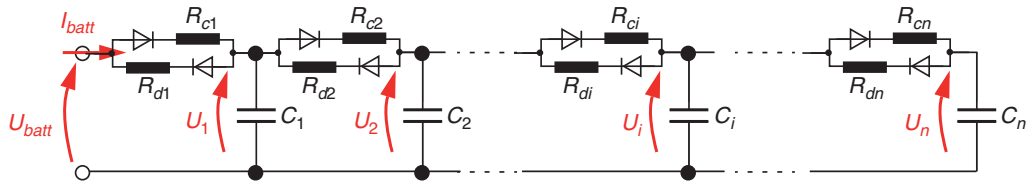

Figure 13

Different resistance values depending on the sign of the current.

where Q is the charge currently stored, $Q_{\min}$ is the charge that remains in the battery when the minimum open circuit voltage $U_{oc,\min}$ is reached, $Q_{\max}$ is the maximum charge that is stored when the battery is at the maximum open circuit voltage $U_{oc,\max}$; C_{batt} is the battery capacitance as calculated in Section 2.3.

The SOC output of the model can be compared to the SOC estimate provided by the BMS. Any difference in SOC due to a bias can be corrected by feeding back ($SOC_{BMS} - SOC$) through an observer gain:

$$\dot{U} = AU + BU_{batt} + H_{SOC}(SOC_{BMS} - SOC) \tag{18}$$

This observer can either correct the voltage of all the capacitors in the model with an H_{SOC} that is a fully populated vector or just the last and largest one with an H_{SOC} that has the structure:

$$H_{SOC} = \left[0 \ \ldots \ 0 \ h_{SOC,n}\right]^T \tag{19}$$

3.2 SOH Observer

State of Health is an indication of the capacity that is still available. This information, provided by the BMS, can be used to adjust all the capacitances of the model:

$$C_{i,corr} = SOH \cdot C_i \tag{20}$$

where SOH is a value in the range [0, 1] *(Ref. [8, 9])*.

3.3 Current or Voltage Observer

For the model with voltage as input and current as output *(Eq. 4 and 5)*, the model output can be compared to the measured current and be used to correct the states of the model. Again, there are several options for its structure. It either can be a "traditional" Luenberger observer with a similar structure as in Equation (18):

$$\dot{U} = AU + BU_{batt} + H_I(I_{batt,meas} - I_{batt}) \tag{21}$$

the gain for such an observer can be designed with any observer design method established in literature. Or it can be an observer that just shuffles charge between the compartments in order to meet the output that is measured. This means that whatever charge is injected in one compartment needs to be removed from another such that the following condition needs to be satisfied:

$$H_I = \left[\frac{h_i}{C_i}\right] \text{with } h_i \text{ such that} \sum_{i=1}^{n} \frac{h_i}{C_i} = 0 \tag{22}$$

For an example where the voltages of the first two compartments should be adjusted and the nth compartment is used to compensate, the gain H_I looks as follows:

$$H_I = \left[\frac{h_1}{C_1} \ \frac{h_2}{C_2} \ 0 \ \ldots \ 0 \ \frac{-(h_1 + h_2)}{C_n}\right]^T \tag{23}$$

For the model with current as input and voltage as output *(Eq. 4, 6 and 7)*, a similar approach is possible. The equivalent to Equation (21) is given by:

$$\dot{U} = AU + BI_{batt} + H_U(U_{batt,meas} - U_{batt}) \tag{24}$$

where again the gain matrix can be designed with any method known in literature. The charge shuffling approach works as well and is the same as for current feedback:

$$H_U = \left[\frac{h_1}{C_1} \ \frac{h_2}{C_2} \ 0 \ \ldots \ 0 \ \frac{-(h_1 + h_2)}{C_n}\right]^T \tag{25}$$

for the same example as above with the first two compartments being corrected.

The first approach (21), (24) amounts to adding or removing charge from the battery; this loss or addition of charge is then corrected by the SOC observer described above in Section 3.1. The second approach (23), (25) does not change the overall charge of the battery such that the SOC is preserved. This approach is especially useful with current as the model input, in which case the SOC value is quite accurate and should not be disturbed.

The effects of the observers can be seen in Figure 14. The green dashed lines show the measured values ($U_{meas} = U_{batt}$ is the input for the model); the solid blue lines are the response the model calculates without use of observers; the red dash-dotted lines are the response with the observers; the model uses four compartments in both cases. The deviation in the calculated current leads to deviations in SOC for the model response. This is corrected with the two observers for SOC and the current.

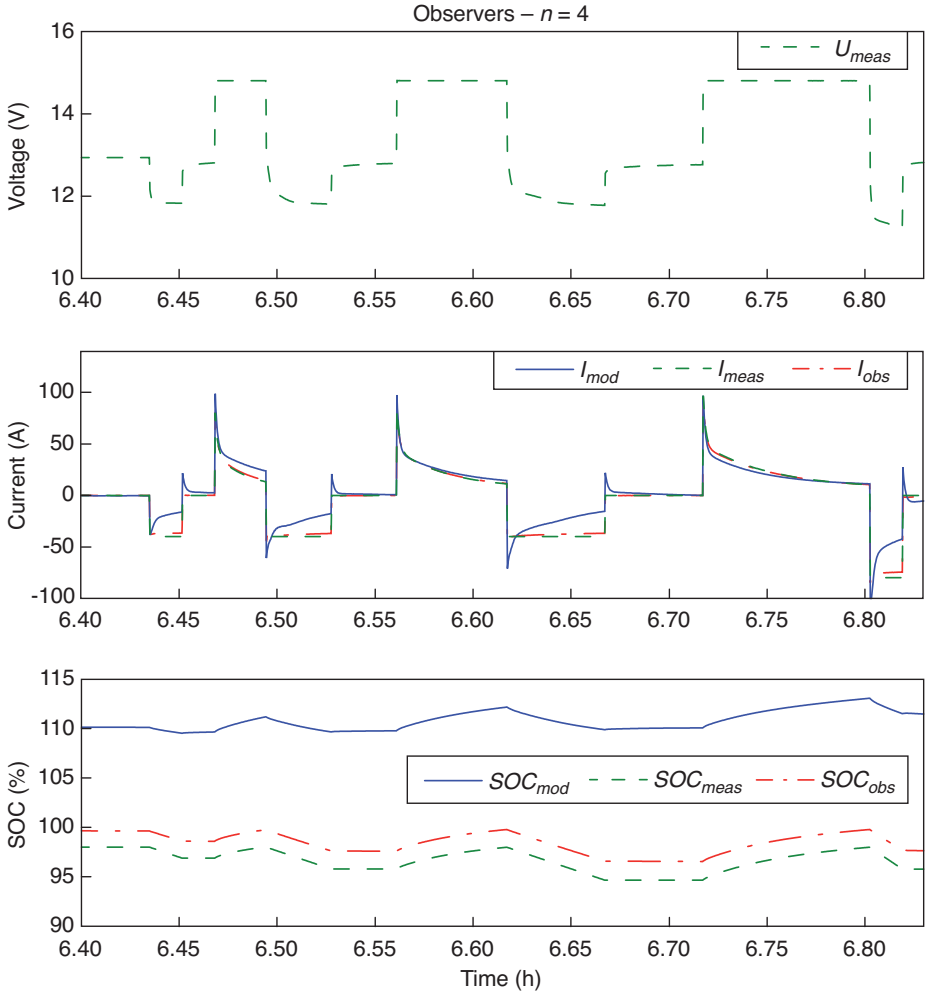

Figure 14

Simulation with observers.

4 ESTIMATOR FOR CHARGE ACCEPTANCE

Now that the model is in place and its states are corrected with the three observers, the charge acceptance can finally be estimated. The mechanism that brings charge into the battery is a voltage applied to the poles that is higher than the internal voltage. This means that some charging voltage $U_{ch} > U_1$ needs to be applied.

The instantaneous charging current the battery would accept for a given charging voltage can thus be calculated in a similar way as the current output (5):

$$I_{CA,\,inst} = \frac{U_{ch} - U_1}{R_1} \tag{26}$$

$I_{CA,inst}$ is the current the battery would accept at any time if the voltage at the poles was set to U_{ch}. This is true during rest, discharge and even during charging with a different voltage than U_{ch}. For instance, Figure 15 shows $I_{CA,inst}$ for rest: it slowly decreases as expected from Phenomenon 6; for discharging where it increases; and for charging with U_{ch}.

Instantaneous charge acceptance only involves the state (voltage) of the first capacitor in the model. When slightly longer term, average charge acceptance should be estimated (*e.g.*, average charging current during the first five seconds of charging with a voltage of U_{ch}), the first few capacitors must be taken into account.

One approach to calculate this averaged charge acceptance in an implementation with a discrete-time version of the model is to simulate the next few seconds at each sampling time. This gives an accurate estimate of the charge acceptance but it is computationally quite involved. Since the

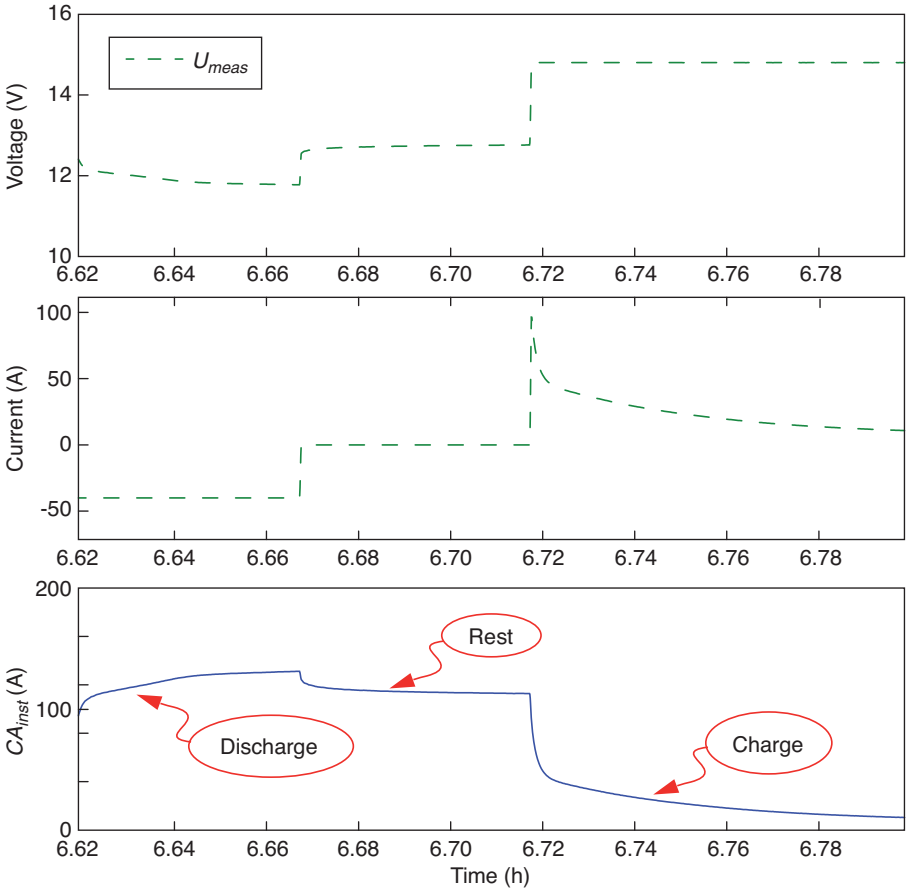

Figure 15

Instantaneous charge acceptance estimation.

applied voltage during charging is assumed to be constant, this simulation is not even necessary. For a discrete-time version of the model that calculates the instantaneous charging current[1]:

$$\begin{bmatrix} U(i+1) \\ I_{CA,\,inst}(i) \end{bmatrix} = \left[\begin{array}{c|c} A_d & B_d \\ \hline C_d & D_d \end{array}\right] \begin{bmatrix} U(i) \\ U_{ch} \end{bmatrix} \tag{27}$$

an additional output for the charge stored during Δt can be constructed (T_s is the sampling time and $k = \Delta t/T_s$):

(see *Eq. 28*)

with Euler forward integration or:

(see *Eq. 29*)

with Euler backward integration; if only very few steps are used for this output (k small), some trapezoidal integration may be more appropriate. The first part in (28) or (29) fed by the state describes the influence of the initial state; the second part the one by the charging voltage. If average charging current rather than cumulated charge should be calculated, the output can be modified:

(see *Eq. 30*)

Since the last compartments do not contribute to the charge acceptance during relatively short times, they could be neglected in the above calculations. However, as it is done offline, it does not harm to simply take the full model. In principle, it is possible to calculate a continuous-time equivalent for Equations (28) or (30) with a structure:

$$\begin{bmatrix} \dot{U} \\ I_{CA,\,inst} \\ I_{CA,\,avg} \end{bmatrix} = \left[\begin{array}{c|c} A & B \\ \hline C_{inst} & D_{inst} \\ C_{avg} & C_{avg}B + D_{avg} \end{array}\right] \begin{bmatrix} U \\ U_{ch} \end{bmatrix} \tag{31}$$

but the final implementation of a charge acceptance estimator will always be in discrete time.

Figure 16 shows average charging current during $\Delta t = 10$ s ("$CA_{\Delta t = 10\text{ s, sim}}$"), together with the instantaneous $I_{CA,\,inst}$ and battery current filtered with moving averaging over 10 s ("$CA_{\Delta t = 10\text{ s, meas}}$"). It is well visible that instantaneous and

(1) This notation is used to represent state space models in a compact form.

$$\begin{bmatrix} \frac{U(i+1)}{I_{CA,\,inst}(i)} \\ \Delta Q_{\Delta t}(i) \end{bmatrix} = \left[\begin{array}{c|c} A_d & B_d \\ \hline C_d & D_d \\ T_s C_d (A_d^{k-1} + \ldots + A_d^2 + A_d + I) & T_s C_d (A_d^{k-2} + 2A_d^{k-3} + \ldots + (k-3)A_d^2 + (k-2)A_d + (k-1)I) B_d + kT_s D_d \end{array}\right] \begin{bmatrix} U(i) \\ \overline{U_{ch}} \end{bmatrix} \tag{28}$$

$$\begin{bmatrix} \frac{U(i+1)}{I_{CA,\,inst}(i)} \\ \Delta Q_{\Delta t}(i) \end{bmatrix} = \left[\begin{array}{c|c} A_d & B_d \\ \hline C_d & D_d \\ T_s C_d (A_d^{k} + \ldots + A_d^2 + A_d) & T_s C_d (A_d^{k-1} + 2A_d^{k-2} + \ldots + (k-2)A_d^2 + (k-1)A_d + kI) B_d + kT_s D_d \end{array}\right] \begin{bmatrix} U(i) \\ \overline{U_{ch}} \end{bmatrix} \tag{29}$$

$$\begin{bmatrix} \frac{U(i+1)}{I_{CA,\,inst}(i)} \\ I_{CA,\,avg}(i) \end{bmatrix} = \left[\begin{array}{c|c} A_d & B_d \\ \hline C_d & D_d \\ \frac{1}{k} C_d (A_d^{k-1} + \ldots + A_d^2 + A_d + I) & \frac{1}{k} C_d (A_d^{k-2} + 2A_d^{k-3} + \ldots + (k-3)A_d^2 + (k-2)A_d + (k-1)I) B_d + D_d \end{array}\right] \begin{bmatrix} U(i) \\ \overline{U_{ch}} \end{bmatrix} \tag{30}$$

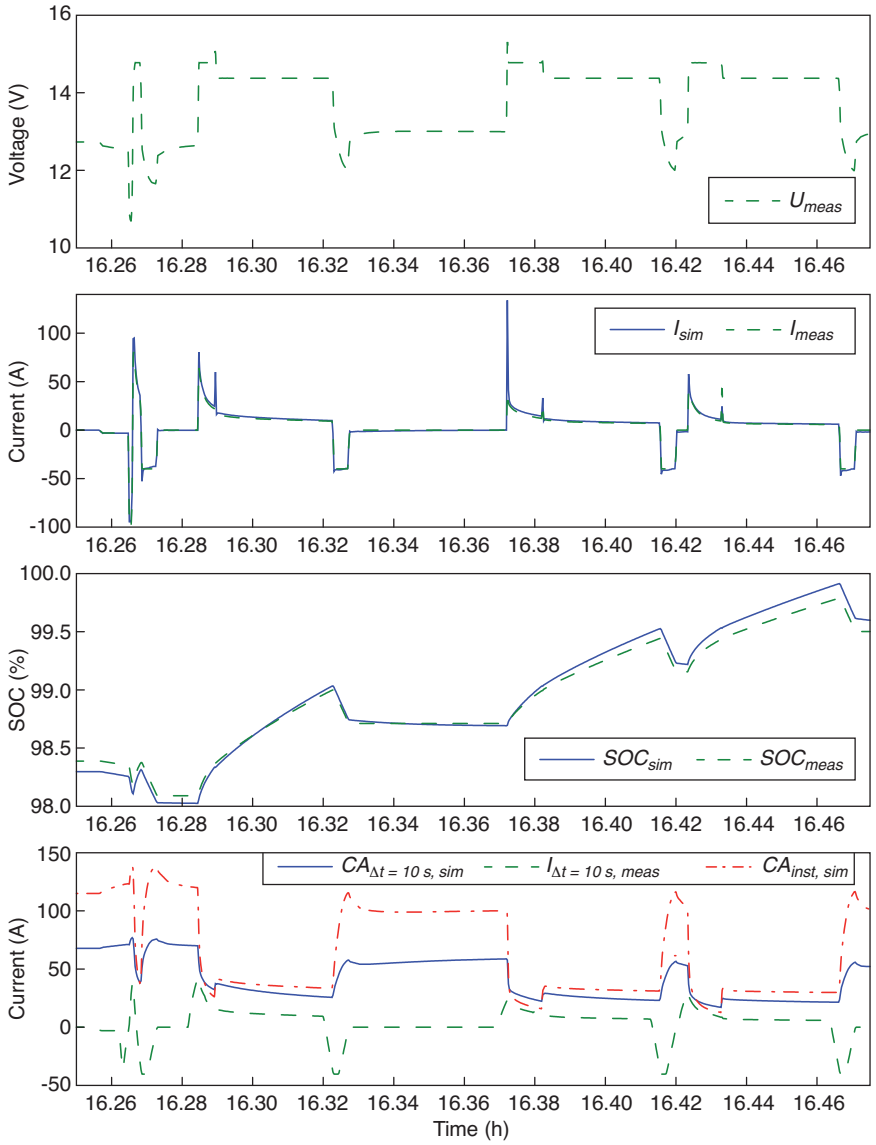

Figure 16

Charge acceptance estimation. $I_{\Delta t = 10\ s,\ meas}$ is the measured current averaged over 10 s.

averaged charge acceptance match quite well during times when the battery is actually charged with U_{ch}. It can also be seen that charge acceptance increases when the battery is charged with a voltage below U_{ch} ($U_{batt} < U_{ch}$).

4.1 Summary: Overall Charge Acceptance Estimator

The model — formulated for current as input —, the observers, and the charging current estimator can now be combined into one set of equations. The inputs for this overall estimator are: I_{batt}, $U_{batt,meas}$, U_{ch}, SOC_{BMS}, ϑ; we neglect the correction of the capacitances by SOH:

(see *Eq. 32*)

where B, C_{avg} and D_{avg} depend on C_i, R_i, Δt. The first line above is simply a reminder that the resistances are temperature dependent. Figure 17 represents this as a block diagram. $U_{oc,\min}$ needs to be fed as a (constant) input in order to obtain an offset in an otherwise linear model.

5 INCLUDING TEMPERATURE DEPENDENCE

The temperature dependence shall be introduced by correcting all terms containing a resistance. Looking at the structure of the model in Equation (32) shows that all nonzero elements of the A matrix of the continuous-time plant model contain a division by one of the resistances. The same is true with the C and D matrix elements associated with the charge acceptance outputs and also with the D matrix element associated with the U_{batt} output. But it is not true with the B matrix, the elements associated with *SOC* of the C and D matrices and with the U_{batt} associated element of the C matrix. The observer gains are uncritical and need not to be corrected for temperature.

All these parts containing a factor $1/R_i$ should be multiplied by the inverse of the polynomial factor introduced in Equation (16). As a polynomial, this factor, $f_\vartheta(\vartheta)$, is described by:

$$f_\vartheta(\vartheta) = b_3\vartheta^3 + b_2\vartheta^2 + b_1\vartheta + b_0 \tag{33}$$

$$R_i = R_i(\vartheta)$$

$$\begin{bmatrix} \dot{U}_1 \\ \dot{U}_2 \\ \vdots \\ \dot{U}_i \\ \vdots \\ \dot{U}_n \end{bmatrix} = \begin{bmatrix} \frac{-1}{C_1R_2} & \frac{1}{C_1R_2} & 0 & 0 & \dots & 0 \\ \frac{1}{C_2R_2} & \frac{-1}{C_2}\left(\frac{1}{R_2}+\frac{1}{R_3}\right) & \frac{1}{C_2R_3} & 0 & \dots & 0 \\ 0 & & \dots & & & 0 \\ 0\dots & \frac{1}{C_iR_i} & \frac{-1}{C_i}\left(\frac{1}{R_i}+\frac{1}{R_{i+1}}\right) & \frac{1}{C_iR_{i+1}} & \dots & 0 \\ 0 & & & \dots & & 0 \\ 0 & & \dots & 0 & \frac{1}{C_nR_n} & \frac{-1}{C_nR_n} \end{bmatrix} \begin{bmatrix} U_1 \\ U_2 \\ \vdots \\ U_i \\ \vdots \\ U_n \end{bmatrix} + \begin{bmatrix} \frac{1}{C_1} \\ 0 \\ \vdots \\ 0 \\ \vdots \\ 0 \end{bmatrix} I_{batt}$$

$$+H_{SOC}(SOC_{BMS} - SOC) + H_U(U_{batt,meas} - U_{batt}) \tag{32}$$

$$U_{batt} = U_1 + R_1 I_{batt}$$

$$SOC = \frac{1}{C_{batt}(U_{oc,\max} - U_{oc,\min})} \sum_{i=1}^{n} C_i(U_i - U_{oc,\min})$$

$$I_{CA,inst} = \frac{U_{ch} - U_1}{R_1}$$

$$I_{CA,avg} = C_{avg}U + (C_{avg}B + D_{avg})U_{ch}$$

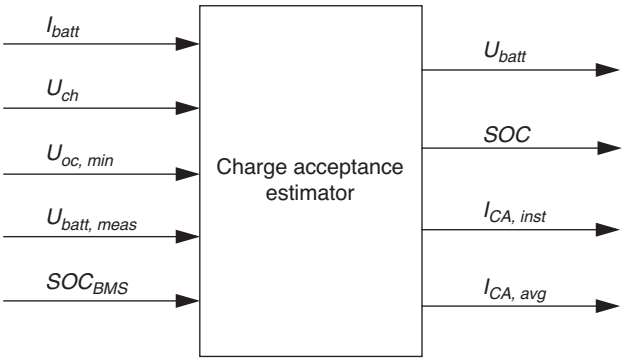

Figure 17

Inputs and outputs of the overall charge acceptance estimator.

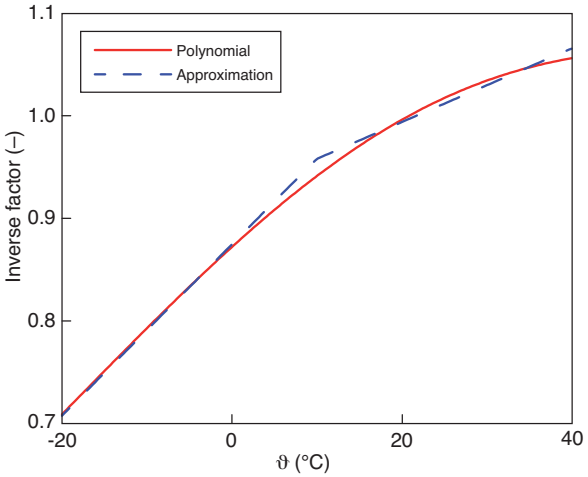

Figure 18

Inverse factor, f_ϑ, modeling temperature dependence.

where the coefficients are $b_3 = -5.1052 \times 10^{-7}$ 1/(°C)^3, $b_2 = -4.9304 \times 10^{-5}$ 1/(°C)^2, $b_1 = 7.3817 \times 10^{-3}$ 1/°C, $b_0 = 0.87181$. Alternatively, since the nonlinearity is rather benign, a linearly interpolating approximation with just two partitions could be used for this (*Fig. 18* and Lookup *Tab. 4*).

TABLE 4

Lookup table for the approximation of temperature dependence

Temperature break points (°C)	–20	10	40
f_ϑ	0.7075	0.9578	1.0654

When discretizing the model, this factor, f_ϑ, is warped, as can be seen from the following approach:

In continuous time, we have:

$$\frac{x_{k+1} - x_k}{T_s} \approx \dot{x} = Ax + Bu \tag{34}$$

where T_s is the sampling time. Hence, the discrete-time form is:

$$x_{k+1} = \underbrace{(I + T_s A)}_{A_d} x_k + \underbrace{T_s B}_{B_d} u_k \tag{35}$$

such that the linear discretized plant model with constant resistances (for $\vartheta = 20$°C),

$$G_{P,\,d} : \begin{cases} x_{k+1} = A_{P,d} x_k + B_{P,d} u_k \\ y_k = C_{P,d} x_k + D_{P,d} u_k \end{cases} \tag{36}$$

where u_k are the inputs and y_k the outputs, can be represented as follows:

$$G_{P,\,LPV} : \begin{cases} x_{k+1} = \left(f_\vartheta (A_{P,\,d} - I) + I\right) x_k + B_{P,\,d} u_k \\ y_k = diag([1\ 1\ \ f_\vartheta\ \ f_\vartheta])\, C_{P,\,d} x_k \\ \qquad + diag\left(\left[\frac{1}{f_\vartheta} 1\ \ f_\vartheta\ \ f_\vartheta\right]\right) D_{P,\,d} u_k \end{cases} \tag{37}$$

In this form, the plant is Linear Parameter Varying (LPV) and it has an additional input, $f_\vartheta(\vartheta)$ or ϑ itself that feeds into the factor f_ϑ.

If the model with U_{batt} as input and I_{batt} as output is used, the corresponding entry in the B matrix needs to be multiplied with the factor f_ϑ as well.

The overall estimator (32), in discretized form, then reads:

$$G_{est,\,LPV} : \begin{cases} U_{k+1} = (f_\vartheta (A_{P,\,d} - I) + I) U_k + B_{P,\,d} I_{batt,\,k} \\ \qquad + T_s H_{SOC} \left(SOC_{BMS,\,k} - \underbrace{\left[0\ 1\ 0\ 0\right](C_{est,\,d} U_k + D_{est,\,d} u_k)}_{SOC_k} \right) \\ \qquad + T_s H_U \left(U_{batt,\,meas,\,k} - \underbrace{\left[1\ 0\ 0\ 0\right](C_{est,\,d} U_k + D_{est,\,d} u_k)}_{U_{batt,\,k}} \right) \\ y_k = diag\left(\left[1\ 1 f_\vartheta\ f_\vartheta\right]\right) C_{est,\,d} U_k \\ \qquad + diag\left(\left[\frac{1}{f_\vartheta} 1 f_\vartheta\ f_\vartheta\right]\right) D_{est,\,d} u_k \end{cases} \tag{38}$$

where U_k is the state; u_k are the inputs and y_k the outputs shown in Figure 17. $C_{est,\,d}$ and $D_{est,\,d}$ are the output matrices of the linear, discrete-time estimator for $\vartheta = 20$°C.

Figure 19 shows simulation results with battery data recorded at –18°C. The battery was subjected to more extreme and more realistic currents in this test: engine cranking pulses with currents of –760 A that lead to voltage drops down to 8 V. As a consequence, the charge acceptance is very high right after these discharge pulses but it decreases quickly at this low temperature.

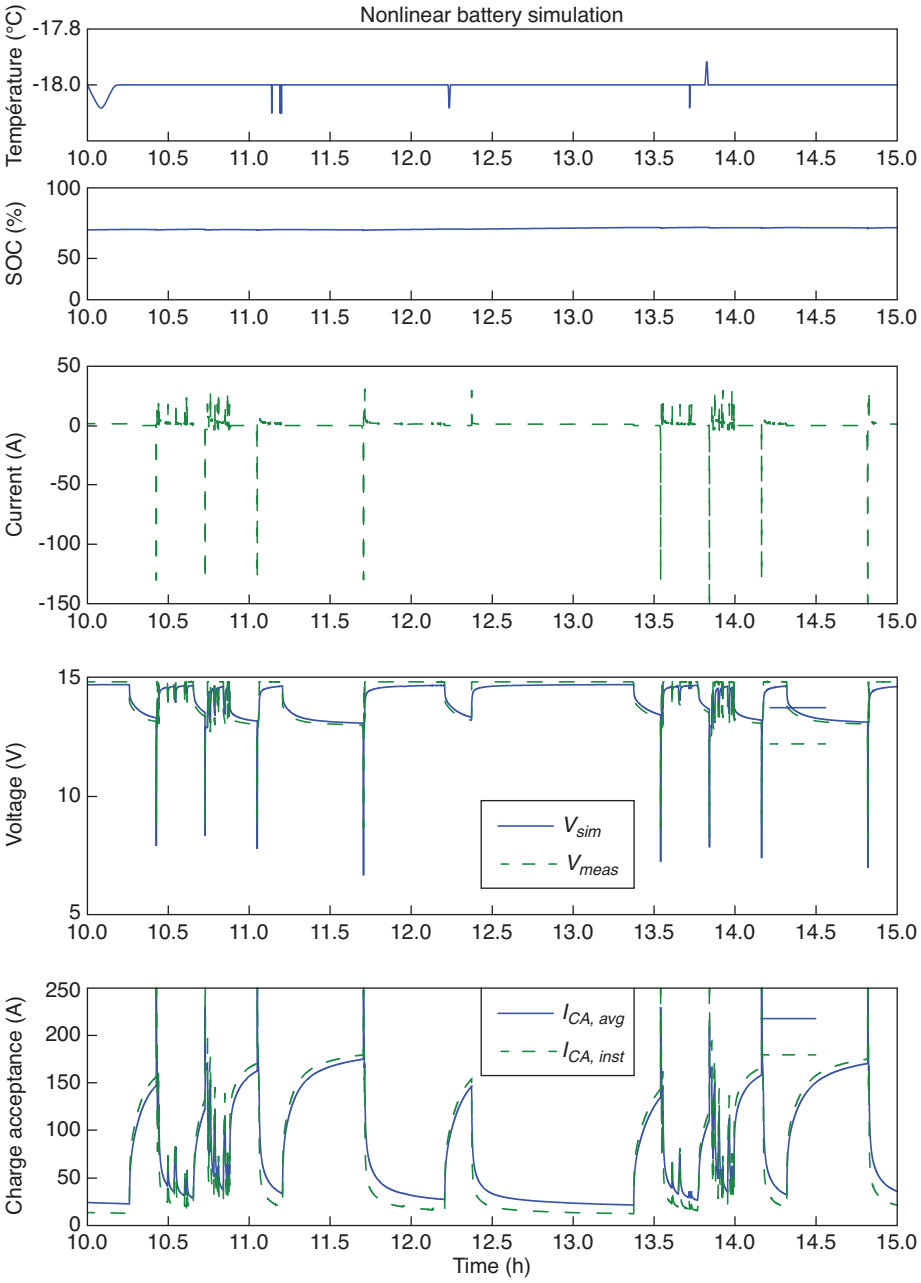

Figure 19

Estimated charge acceptance with data recorded at low temperature.

CONCLUSION

This paper describes the phenomena to be captured and an estimator for charge acceptance of lead acid batteries. The estimator is based on the approximation of a model using a partial differential equation that allows for representing a wide range of time constants. Since the model is essentially linear — the only nonlinearity enters through the temperature dependence of the equivalent resistors and varies in much larger time frames than the prediction horizon for charge acceptance — the actual estimator can be formulated in closed form. Additional observers help to improve the prediction quality.

For implementation in an automotive control system such a phenomenological model is more suitable than physics and chemistry based ones. The availability of such a model in the vehicle allows for a more efficient management of battery and thus to reduce the fuel consumption for charging.

ACKNOWLEDGMENTS

Thanks to Ralf Hecke for the numerous clarifying discussions and to Christoph Arndt who was always available for the more philosophical discussions.

This work was partially supported by the European Commission through project MOBYDIC (FP7-INFSO-ICT-248858), http://www.mobydic-project.eu.

REFERENCES

1 Chaturvedi N.A., Klein R., Christensen J., Ahmed J., Kojic A. (2010) Algorithms for advanced battery-management systems. Modeling, estimation, and control challenges for Lithium-ion batteries, *IEEE Control Syst. Mag.* **30**, 3, 49-68, DOI: 10.1109/MCS.2010.936293.

2 Thele M., Karden E., Surewaard E., Sauer D.U. (2006) Impedance-based overcharging and gassing model for VRLA/AGM batteries, *J. Power Sources* **158**, 953-963, DOI: 10.1016/j.jpowsour.2005.11.025.

3 Sauer D.U., Karden E., Fricke B., Blanke H., Thele M., Bohlen O., Schiffer J., Gerschler J.B., Kaiser R. (2007) Charging performance of automotive batteries – an underestimated factor influencing lifetime and reliable battery operation, *J. Power Sources* **168**, 22-30, DOI: 10.1016/j.jpowsour.2006.11.064.

4 Tenno A. (2004) Modelling and evaluation of valve-regulated lead-acid batteries, *PhD Dissertation*, Helsinki University of Technology.

5 Ceraolo M. (2000) Dynamical models of lead-acid batteries, *IEEE Trans. Power Syst.* **15**, 1184-1190.

6 Jackey R.A. (2007) A simple, effective lead-acid battery modeling process for electrical system component selection, *SAE Technical Paper* 2007-01-0778.

7 Vasebi A., Bathaee S.M.T., Partovibakhsh M. (2008) Predicting state of charge of lead-acid batteries for hybrid electric vehicles by extended Kalman filter, *Energy Convers. Manage.* **49**, 75-82.

8 Karden E., Spijker E., Kok D., Kees D. (2003) In-vehicle battery management for high-volume applications, *Elektronik im Kraftfahrzeug 2003*, VDI Berichte, Vol. 1789, ISBN 3-18-091789-X, pp. 963-987.

9 Meissner E., Richter G. (2003) Battery monitoring and electrical energy management precondition for future vehicle electric power systems, *J. Power Sources* **116**, 79-98, DOI: 10.1016/S0378-7753(02)00713-9.

10 Schaeck S., Stoermer A.O., Kaiser F., Koehler L., Albers J., Kabza H. (2011) Lead-acid batteries in micro-hybrid applications. Part I. Selected key parameters, *J. Power Sources* **196**, 3, 1541-1554, DOI:10.1016/j.powsour.2010.08.077.

11 Parodi M., Storace M., Cincotti S. (1996) Static and dynamic hysteretic features in a PWL circuit, *Int. J. Circuit Theory Appl.* **24**, 183-199.

Final manuscript received in January 2012
Published online in July 2012

Copyright © 2012 IFP Energies nouvelles

Permission to make digital or hard copies of part or all of this work for personal or classroom use is granted without fee provided that copies are not made or distributed for profit or commercial advantage and that copies bear this notice and the full citation on the first page. Copyrights for components of this work owned by others than IFP Energies nouvelles must be honored. Abstracting with credit is permitted. To copy otherwise, to republish, to post on servers, or to redistribute to lists, requires prior specific permission and/or a fee: Request permission from Information Mission, IFP Energies nouvelles, fax. +33 1 47 52 70 96, or revueogst@ifpen.fr.